

Cation- π Interactions As Lipid-Specific Anchors for Phosphatidylinositol-Specific Phospholipase C

Cédric Grauffel,^{†,‡} Boqian Yang,^{§,||} Tao He,^{||} Mary F. Roberts,^{||} Anne Gershenson,[§] and Nathalie Reuter^{*,†,‡}

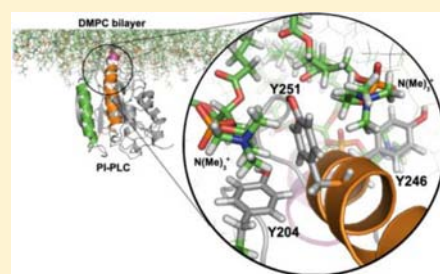
[†]Department of Molecular Biology and [‡]Computational Biology Unit, UniResearch, University of Bergen, Bergen, Norway

[§]Department of Biochemistry and Molecular Biology, University of Massachusetts, Amherst, Massachusetts, United States

^{||}Department of Chemistry, Boston College, Chestnut Hill, Massachusetts, United States

S Supporting Information

ABSTRACT: Amphitropic proteins, such as the virulence factor phosphatidylinositol-specific phospholipase C (PI-PLC) from *Bacillus thuringiensis*, often depend on lipid-specific recognition of target membranes. However, the recognition mechanisms for zwitterionic lipids, such as phosphatidylcholine, which is enriched in the outer leaflet of eukaryotic cells, are not well understood. A 500 ns long molecular dynamics simulation of PI-PLC at the surface of a lipid bilayer revealed a strikingly high number of interactions between tyrosines at the interfacial binding site and lipid choline groups with structures characteristic of cation- π interactions. Membrane affinities of PI-PLC tyrosine variants mostly tracked the simulation results, falling into two classes: (i) those with minor losses in affinity, $K_d(\text{mutant})/K_d(\text{wild-type}) \leq 5$ and (ii) those where the apparent K_d was 50–200 times higher than wild-type. Estimating $\Delta\Delta G$ for these Tyr/PC interactions from the apparent K_d values reveals that the free energy associated with class I is ~ 1 kcal/mol, comparable to the value predicted by the Wimley–White hydrophobicity scale. In contrast, removal of class II tyrosines has a higher energy cost: ~ 2.5 kcal/mol toward pure PC vesicles. These higher energies correlate well with the occupancy of the cation- π adducts throughout the MD simulation. Together, these results strongly indicate that PI-PLC interacts with PC headgroups via cation- π interactions with tyrosine residues and suggest that cation- π interactions at the interface may be a mechanism for specific lipid recognition by amphitropic and membrane proteins.



INTRODUCTION

Cation- π interactions are ubiquitous noncovalent interactions that can be energetically equivalent or stronger than hydrogen bonds.^{1,2} In proteins cation- π interactions are a driving force for structure formation and stability as well as function^{1,3} and are typically observed between aromatic amino acids (phenylalanine, tryptophan, histidine, or tyrosine) and ammonium or guanidinium groups from lysines and arginines, respectively.⁴ Cation- π interactions are also important for substrate and ligand binding, particularly for molecules containing a choline group,^{5–9} as observed, for example, in the X-ray structure of the human phosphatidylcholine transfer protein (PC-TP),⁵ where the choline moiety of the lipid substrate is involved in cation- π interactions within a cage of three tyrosine residues.

Cation- π interactions with lipids in cell membranes have been suggested to play a role in the structural stability and lipid specificity of integral membrane proteins. In molecular dynamics (MD) simulations of the gramicidin (gA) dimer, as a model for membrane-spanning proteins containing interfacial Trp residues, Petersen and co-workers show that phosphatidylethanolamine (PE) and, to a lesser extent, phosphatidylcholine (PC) interact with interfacial tryptophans via cation- π interactions.¹⁰ Trp involvement in cation- π interactions with the membrane has also been observed in other simulations, for

short peptides^{11,12} and for an amphitropic enzyme.¹³ Combined NMR and modeling studies on small model systems describe the interactions between choline-containing lipid headgroups and indole groups as complex and involving cation- π interactions, hydrogen bonds, and carbonyl-cation interactions.^{10,14,15} The available literature thus strongly suggests that cation- π interactions mediated by protein indole groups can play an important role in protein-lipid interfacial binding and lipid specificity. Although tyrosine residues can in principle engage in cation- π interactions with choline-containing lipids,¹⁵ much less is known about these contributions to membrane binding by proteins.

Unlike integral membrane proteins, amphitropic proteins do not span the lipid bilayer, and their affinity for cell membranes is mostly accounted for by their interactions with the lipid headgroups. They bind at the surface of cell or organelle membranes in order to perform their function. Examples include cytochrome P450 and annexins as well as phospholipases, and many of these protein-membrane interactions facilitate cellular reactions to environmental changes.¹⁶ Amphitropic proteins bind reversibly to lipid vesicles with

Received: December 28, 2012

Published: March 18, 2013

equilibrium association constants typically between 10^3 and 10^7 M^{-1} .¹⁶ Electrostatic interactions drive their positioning and orientation at the membrane surface thus facilitating the intercalation of a few hydrophobic groups. It is generally acknowledged that the association of amphitropic proteins with lipid bilayers is fast, while the dissociation is slow; the dissociation rate constant is thus the main determinant of the binding strength. As a consequence, in simple systems where the protein does not undergo conformational changes and does not interact with other proteins, the affinity for the membrane is mostly accounted for by interactions between the protein interfacial binding site and lipids. The energy and specificity of these interactions are generally estimated by including contributions from electrostatics, ~ -1.4 kcal/mol for each positively charged amino acid interacting with the lipid headgroups,¹⁷ and hydrophobic interactions with the bilayer core, ~ -0.8 kcal/mol per acyl chain CH_2 group interacting with the protein.¹⁸ However, as we have seen above, electrostatic interactions with lipid headgroups may not necessarily be restricted to charged amino acids and hydrogen bonds. It is thus possible that interfacial cation- π interactions between aromatic residues and lipids have been overlooked for amphitropic proteins.

To investigate the possible role of cation- π interactions in the binding of amphitropic proteins to membranes, we used a combination of MD simulations, including explicit lipid bilayers, and experimental measurements of membrane binding using fluorescence correlation spectroscopy (FCS). *Bacillus thuringiensis* phosphatidylinositol specific phospholipase C (PI-PLC) was chosen as a model system because it is activated by binding to membranes containing PC or sphingomyelin, and a number of Trp and Tyr residues have been implicated in PC binding.^{19–22} This system also allows facile testing of the simulation results by generating mutant PI-PLCs lacking one or more Tyr residue.

In what follows we present a combined *in silico* and *in vitro* study of the binding to PC-rich bilayers of the wild-type (WT) enzyme and 11 tyrosine mutants (7 single and 4 double mutants). We first describe the analysis of a 500 ns MD simulation of the WT enzyme in a bilayer containing 256 dimyristoylphosphatidylcholine (DMPC) lipids using the Charmm36 force field.²³ The trajectory obtained is analyzed to inventory protein-lipid interactions at the interfacial binding site and in particular the interactions involving interfacial aromatic amino acids. Next we present the results of experiments prompted by the results of the MD simulations. The binding of the WT enzyme and tyrosine mutants to small unilamellar vesicles (SUVs) was measured using FCS, and the severity of binding defects was evaluated by comparison to WT PI-PLC. With only one exception, Tyr residues with long-lived cation- π interactions in the simulations showed the most severe binding defects. The results also indicate that two Tyr residues may cooperatively form adducts with the same lipid headgroup. We finally present a semiquantitative analysis of how tyrosine-choline cation- π interactions contribute to PI-PLC membrane binding affinity.

RESULTS

PI-PLC specifically cleaves the *sn*-3 phosphodiester bond in phosphatidylinositol (PI). While eukaryotic PI-PLCs are usually multidomain proteins containing both membrane binding (PH and C2 domains) and catalytic domains, the bacterial enzymes combine membrane binding and catalytic activity in a single $\alpha\beta$

barrel. The well-studied *B. thuringiensis* PI-PLC is a 34.8 kDa secreted protein that targets eukaryotic cells and, like many other bacterial PI-PLC enzymes, likely plays a role in bacterial virulence. It folds to a distorted ($\alpha\beta$)₈-barrel²⁴ structure and anchors to lipid bilayers via a small α -helix (helix B) as well as neighboring loops and two longer α -helices, F and G,^{19–22} regions that contain at least eight tyrosines (Tyr) and two tryptophans (Trp) (Figure 1). These aromatic amino acids are

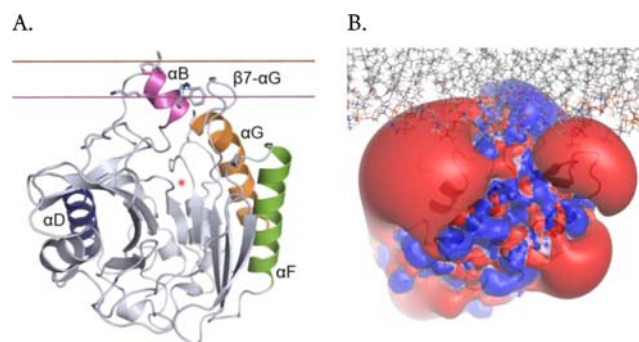


Figure 1. PI-PLC membrane binding orientations from MD simulations. (A) IMM1 orientation of PI-PLC used to initiate the simulations with explicit lipids. Helices B, D, F, and G are magenta, blue, green, and orange, respectively. The active site is represented by a red fuzzy dot. (B) Positioning of PI-PLC in the explicit bilayer model. Lipids are represented with thin sticks colored according to the atomic elements (N: blue, O: red, P: orange, C and H: gray). Electrostatic potential of PI-PLC; the equipotential contours at ± 1 kT (red/blue) calculated using APBS.²⁵ The potential between -1 and $+1$ kT is mapped on the molecular surface (negative: red, positive: blue).

associated with tighter binding of *B. thuringiensis* PI-PLC to PC containing membranes and the activation of substrate cleavage by membranes containing 0.1–0.5 mol fraction PC (X_{PC}) suggests that this *Bacillus* PI-PLC specifically recognizes PC headgroups.^{19,21,22}

Docking PI-PLC to an Anionic Implicit Membrane Model. Experimental data²¹ indicate that PI-PLC interacts with phospholipid bilayers via helix B and surrounding loops. Yet, there is no direct structural data showing PI-PLC bound to lipid layers. To initiate all-atoms MD simulations we therefore had to generate a model of the membrane bound form of PI-PLC. Electrostatic interactions between PI-PLC and membranes are relatively weak, as mutagenesis of a single Lys residue to Ala (K44A) is sufficient to increase the apparent K_d toward PC containing vesicles by at least 2 orders of magnitude.²¹ We therefore did not expect to be able to observe spontaneous binding of PI-PLC to the membrane using all atoms simulations within tractable time scales (unlike what has been observed for other proteins with strong electrostatic binding).²⁶ We used simulations with an implicit membrane model (IMM1-GC)^{27,28} to determine the initial orientation of PI-PLC relative to the membrane, allowing a more cost-effective exploration of potential interface binding sites on the protein surface.

Simulations using anionic implicit membranes were initiated using six PI-PLC orientations relative to the membrane. Each of these orientations corresponds to one face of a cube containing the enzyme. Half (3/6) of these orientations led to an anchored PI-PLC at the model membrane. In the corresponding nine simulations (three for each initial orientation), the anchorage is

Table 1. Anchorage of PI-PLC in DMPC Lipids: Depth and Inventory of Interactions

SSE ^a	aa no.	depth ^b (Å)	hydrophobic ^c	H-bonds ^d (%)	cations- π ^e (%)	
α B	Q40	0.6 ± 2.3	2.1	98.1/34.0		
	N41	3.3 ± 1.8	1.4	97.0/55.1		
	P42	4.2 ± 1.9	5.7			
	I43	4.3 ± 1.7	7.7			
	K44	0.4 ± 1.7	2.5	99.0		
	Q45	-0.6 ± 1.9		32.8		
	V46	0.4 ± 1.9	4.7			
	W47	-0.8 ± 1.9	3.0			
β 2	R71	-10.1 ± 2.0		50.3		
β 2- α D	P84	-3.2 ± 1.9	2.9			
	L85	-3.6 ± 1.6	1.9			
	Y86	-5.5 ± 1.9	1.0	30.1	22.5	
	Y88	-4.9 ± 2.0		58.1	95.6	
β 3- α E	Y118	-8.7 ± 2.1		47.9	23.8	
	K122	-6.1 ± 2.9		54.7		
β 6- α F	Y200	-10.9 ± 2.2			64.4	
	K201	-7.6 ± 2.6		53.4		
α F	Y204	-7.3 ± 2.6			25.2	
β 7- α G	S236	-6.6 ± 2.0		51.9		
	S237	-3.0 ± 1.9	1.3			
	G238	0.1 ± 2.0	1.1			
	G239	2.2 ± 1.9	3.4			
	T240	3.3 ± 2.0	2.6			
	A241	2.6 ± 2.2	3.0			
	W242	3.9 ± 2.4	3.0			
	N243	-0.3 ± 2.3		39.0		
	S244	-2.3 ± 2.1		75.2		
	α G	Y246	-4.5 ± 2.4		38.7	77.3
		Y247	-2.3 ± 2.5		44.6	8.9
S250		-7.2 ± 2.7		24.1		
	Y251	-6.7 ± 3.2		25.8	36.7	
	K279	-8.1 ± 3.1		19.6		

^aSecondary structure elements; α : helix, β : strand, β i- α X: loop between strand i and helix X. ^bMean values and standard deviations. Positive values indicate that the center of mass of the amino acid is buried in the bilayer, beyond the plane defined by the phosphate groups. ^cAverage number of hydrophobic contacts per frame (listed if >1). ^dOccupancies of hydrogen bonds in % (if >20; bold numbers for backbone hydrogen bonds). ^eOccupancy of cation- π adducts (if >10%).

always achieved via helix B (cf. Figure 1) in agreement with published experimental data.²¹

The simulation yielding the lowest IMM1-GC effective energy was selected for further analysis. The average binding energy (ΔW) calculated for the last 1.5 ns of this simulation is -5.6 ± 1.0 kcal/mol. Decomposition of the binding energy shows that the largest contributions arise from hydrophobic interactions with residues in helix B. Interestingly, despite the proximity of interfacial Tyr residues to the membrane plane, these residues show no significant energetically favorable interactions of Trp or Tyr residues with the implicit membrane (a detailed list of all favorable contributions is provided as Supporting Information). This is similar to what we observed for another amphitropic protein, proteinase 3, where a tryptophan residue (Trp218) did not significantly contribute to binding in IMM1 simulations,²⁹ but all-atom simulations¹³ revealed its involvement in hydrogen bonds and cation- π interactions with the carbonyl and choline moieties of DMPC lipids. Although the implicit membrane model is useful for predicting the correct orientation of PI-PLC at the membrane, in our experience it underestimates the interfacial interactions of aromatic amino acids.

Simulation of PI-PLC Interactions with DMPC Bilayers.

The orientation of PI-PLC predicted by the implicit membrane simulations was used to initiate simulations of the protein with an all-atom lipid bilayer model. Although the binding of PI-PLC is strongest in PC/PG mixtures, we chose to use pure DMPC bilayers to avoid artifacts due to the initial positioning of neutral lipids with respect to the protein.

PI-PLC exhibits very little structural change during the 500 ns MD simulation. The root-mean-square deviation (RMSD) of the backbone atoms is on average low (1.4 Å) and stays stable throughout the simulation. A plot of the RMSD time evolution is provided as Supporting Information. We evaluated the amino acid anchorage depth at the interfacial binding site (IBS) by calculating the distance between the residue centers of mass and the average plane defined by the position of the phosphorus atoms. This distance was calculated for every frame in the trajectory and averaged. Results are reported in Table 1, where the list of amino acids is sorted by structural elements, and in the Supporting Information. The most deeply buried amino acids are located on helix B (Ile43, Pro42, Asn41) and on the β 7- α G loop (Trp242, Thr240, Ala241, Gly239). These residues penetrate 2–4 Å, on average, inside the plane defined by the phosphorus atoms. Other amino acids of the IBS, such

as tyrosines, are situated on the other side of the phosphate plane.

Interactions between PI-PLC residues and membrane lipids were monitored during the MD simulation, and the most frequent ones are reported in Table 1. For each amino acid, we report the average number of hydrophobic contacts per frame, occupancies of hydrogen bonds, and cation- π interactions. The criteria for detection of the interacting pairs are given in the Methods section. The geometry of the PI-PLC binding region after 300 ns of simulation is shown in Figure 2 where we

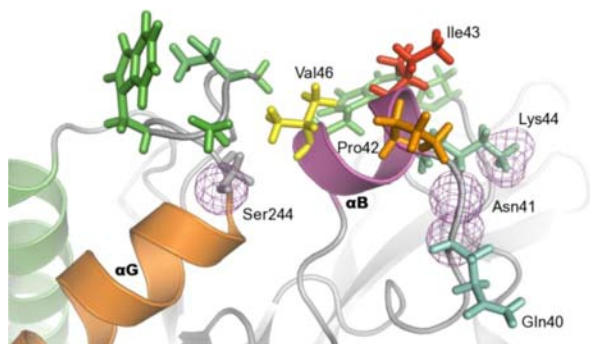


Figure 2. PI-PLC amino acids involved in hydrogen bonds and hydrophobic contacts with DMPC lipids. The structure of PI-PLC after 300 ns is represented with cartoons. The side chains of amino acids involved in long-lasting hydrogen bonds (occupancies >75%) are represented with a pink mesh, while those involved in hydrophobic contacts (if average number of contacts per frame >2) are represented with sticks and colored following a cyan (equal to 2) to red (equal to 8) gradient.

highlight the amino acid side chains involved in hydrophobic contacts with the lipid tails (for those with an average number of contacts per frame >1). Ile43 in helix B has the highest number of hydrophobic contacts, consistent with it being the most deeply buried residue in PI-PLC. In addition, each of the helix B hydrophobic side chains (Pro42, Ile43, Val46) is in contact with more than one lipid hydrophobic group, and these contacts remain throughout most of the simulation.

Other regions of the enzyme are also in contact with hydrophobic lipid tails, although they are less deeply buried than Ile43. This is the case for residues in the loop between the second strand of the β barrel ($\beta 2$) and helix D. This long (>15 aa) loop contains the catalytic residue His82 and is partially structured in two short strands. Pro84, Leu85, and Tyr86 from this loop are in contact with the hydrophobic lipid tails during most of the simulation time. The contacts from Pro84 and Leu85 have occupancies >75%, while Tyr86 has an occupancy of 30%. Only one other structural element, the loop preceding helix G (Ser237 to Trp242) is involved in hydrophobic contacts with the lipid tails. Hydrophobic intercalation is thus restricted to three regions of *B. thuringiensis* PI-PLC: helix B, the $\beta 2$ -helix D loop, and the $\beta 7$ -helix G loop.

Most hydrogen bonds between the protein and the membrane involve phosphate groups. From Table 1 one can see that a few amino acid residues in helix B and the $\beta 7$ -helix G loop achieves long-lasting hydrogen bonds with occupancy >70%, while the other structural elements have shorter-lived interactions. Interestingly Gln40 and Asn41 interact through their backbone atoms. The side chains of Lys44, Ser244 and Asn41 also mediate long-lasting hydrogen bonds. Tyr86 is the other residue involved in a backbone mediated hydrogen bond,

but to a lesser extent. $\beta 2$ is involved via Arg71 and the subsequent loop carrying Tyr88. Two other loops, $\beta 3$ -helix E and $\beta 6$ -helix F, interact with phosphate groups via Lys122 and Lys201, respectively.

The frequency of aromatic amino acids, especially tyrosines, at the interface between PI-PLC and the membrane is strikingly high. We screened the trajectory frames to identify potential cation- π interactions between choline and aromatic (Trp indole or Tyr phenol) groups, using a geometric criteria (see Methods section). Figure 3A shows the time evolution of these

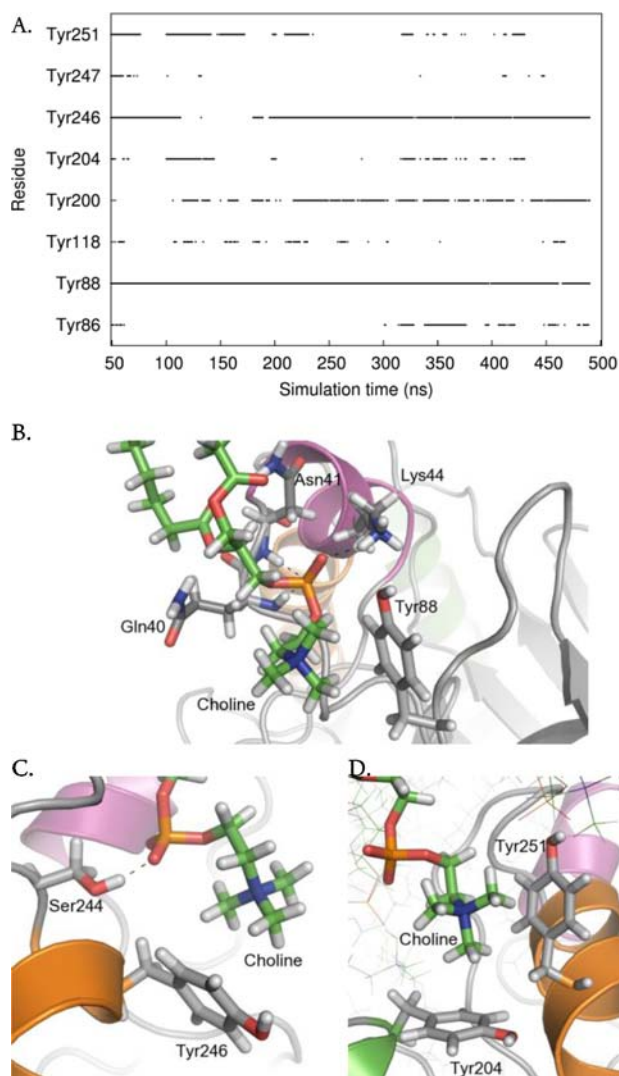


Figure 3. Cation- π interactions identified during the simulation. (A) Occurrences of cation- π interactions for aromatic residues versus simulation time (occupancies >5%). (B-D) Snapshots of cation- π interactions collected along the simulation (representative frames taken between 400 and 500 ns). Color code for cartoons as in Figure 1A.

interactions, while snapshots of such choline-tyrosine interactions are highlighted in Figures 3B-D. It is interesting to note that some tyrosine side chains seem to undergo significant changes of their orientation compared to the starting structure due to interaction with lipids. Our analysis reveals that three tyrosines are involved in very long-lasting cation- π interactions (>50% lifetime): Tyr88, Tyr200, and Tyr246.

Interestingly, cation- π interactions of Tyr88 and Tyr246 engage the same lipids as the longest-lasting hydrogen bonds. The phospholipid, the head of which is involved in a cation- π interaction with Tyr88, is also hydrogen bonded via its phosphate to the Lys44 side chain and the backbone of Gln40 and Asn41 (Figure 3B). Tyr246 (cation- π) and Ser244 (hydrogen bond) also share the same partner ~60% of the time. The corresponding arrangement of the two amino acids and a lipid is illustrated in Figure 3C. It is worth noting that the hydrogen bonds described are not present in the starting structure and are formed during the first 50 ns of simulation. Unlike Tyr88 and Tyr246, the cation- π interactions involving Tyr200 are not interfacial. Tyr200 is the most distant of the three from the membrane, and it forms an interaction with the choline group of a lipid that sticks out of the bilayer halfway into the active site.

Four other tyrosines are involved in less stable cation- π interactions (occupancy from 20 to 40%) that nevertheless occur regularly throughout the simulation: Tyr86, Tyr118, Tyr204, and Tyr251. A few other aromatic amino acids are observed mediating cation- π interactions with choline groups, but these are less frequent events: Tyr53 (2.5%), Tyr247 (8.9%), and Tyr248 (1.9%). In our simulations, all significant cation- π interactions with cholines are thus mediated by tyrosines, while tryptophans interact with the lipid tails (compare the inventory of hydrophobic contacts in Table 1).

Among the four tyrosines (246, 247, 248, 251) in helix G, three are involved in cation- π interactions and two of them (246 and 251) rather strongly. Because of their consecutive location on an α -helix, the side chains of tyrosines 246, 247, and 248 point in different directions and interact with different lipids.

In contrast, the side chains of Tyr247 and Tyr251 are on the same side of the helix, separated by one turn, and these residues can interact with the same lipid choline group. Similarly, the orientation of Tyr204 on helix F and Tyr251 on helix G allows simultaneous interactions with the same lipid. Tyr247 is involved in cation- π interactions with choline headgroups only 8.9% of the time, but for about half of these interactions (~5% of the simulation time) Tyr251 is also interacting with this headgroup (Figure 3A). More frequently, 14.3% of the time, Tyr204 and Tyr251 are involved in cation- π interactions with the same choline headgroup (Figure 3D), and this lipid is distinct from that interacting with Tyr247. This correlation between Tyr204 and Tyr251 lipid binding is reflected in Figure 3A and is in agreement with a study using a combination of high-resolution field-cycling ^{31}P NMR and molecular docking that implicated both 204 and 251 in a tight PC binding site in *B. thuringiensis* PI-PLC.³⁰ In our simulations, we never observe more than two tyrosines simultaneously interacting with the same lipid. Yet homologues to Y204, Y247, and Y251 are shown to be involved in choline binding in a recent X-ray crystal structure of a *Staphylococcus aureus* PI-PLC variant with two introduced Tyr residues.³¹

Unlike the other Tyr residues at the top of helix G, Tyr248 is almost never involved in interactions with lipids (cation- π occupancy: 1.9%, hydrogen bonds <10%). It instead engages in long-lived intramolecular hydrophobic interactions with Leu235 and Pro245 which appear to maintain the structure and orientation of the rim loop between β 7 and helix G. The hydrogen bond between the backbone nitrogen of Asn243 and the backbone oxygen of Gly238 also helps stabilize the shape of this loop. Figure 4 shows the difference between structures of

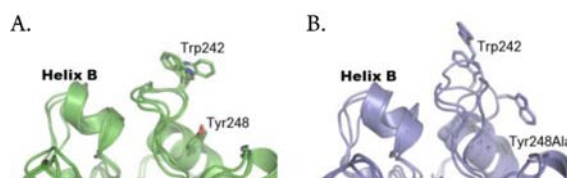


Figure 4. Effect of the Y248A mutation on PI-PLC. Structure of the interfacial binding sites of (A) WT PI-PLC and (B) Y248A after 20 ns MD simulations in water, from three independent simulations in each case.

Tyr248Ala mutants and WT obtained from MD simulations in water (Figure 4). In the mutant simulations the rim loop is more flexible, and the distance to helix B increases. Accordingly there is a significant increase in the atomic fluctuations of both the rim loop and helix B (root-mean-square fluctuations are provided as Supporting Information). The simulations thus indicate that the role of Tyr248 in membrane binding is to restrict PI-PLC conformational space rather than making direct contacts with the lipids.

Effects of Tyr Mutations on PI-PLC Binding to Small Unilamellar Vesicles (SUVs). The MD simulations with an explicit DMPC membrane identify Tyr residues in the loop between β 2 and helix D (86, 88), in helix F (204), and in helix G (246–247, 251) as important for cation- π interactions with PC headgroups. Tyr248, also at the interfacial binding site, seems to have a slightly different role. These predictions were tested using single or double Tyr mutants of PI-PLC and measuring protein binding to SUVs using FCS. Because *B. thuringiensis* PI-PLC binding to SUVs is synergistic, with lower affinity for SUVs composed only of anionic lipids or pure PC SUVs,^{21,32} binding was measured as a function of mole fraction PC (X_{PC}) for phosphatidylglycerol (PG) SUVs. The anionic lipid PG was used as a substrate analog because the production of diacylglycerol from PI would lead to vesicle fusion compromising FCS binding experiments. Apparent K_{d} s and apparent K_{d} s relative to WT are plotted in Figure 5 as a function of X_{PC} . Values of apparent K_{d} s at $X_{\text{PC}} = 1$ are given in Table 2.

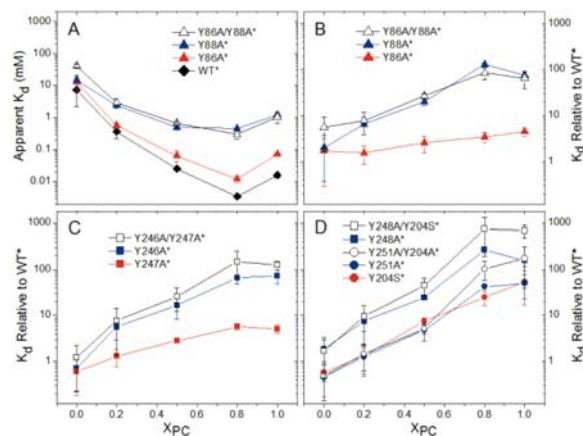


Figure 5. Binding of PI-PLC Tyr variants to SUVs. (A) Apparent K_{d} and (B–D) apparent K_{d} relative to WT* as a function of X_{PC} . The error bars are the largest uncertainties generated during the FCS data analysis, either the standard deviations from two independent repeats or the uncertainty generated by error propagation for the two independent data sets.

Table 2. Apparent K_d Values of Mutants of *B. thuringiensis* PI-PLC Variants Towards Pure PC SUVs ($X_{PC} = 1$)

mutant	apparent K_d (mM) ^a
WT*	0.016 ± 0.003
Y86A*	0.072 ± 0.005
Y88A*	1.2 ± 0.1
Y204S*	0.87 ± 0.58
Y246A*	1.2 ± 0.3
Y247A*	0.082 ± 0.007
Y248A*	2.5 ± 0.5
Y251A*	0.81 ± 0.41
Y86A/Y88A*	1.1 ± 0.4
Y246A/Y247A*	2.0 ± 0.1
Y248A/Y204S*	11 ± 3
Y251A/Y204A*	2.8 ± 2.1

^aThe uncertainties are the largest uncertainties generated during the FCS data analysis, either the standard deviations from two independent repeats or the uncertainty generated by error propagation for the two independent data sets.

None of the single Tyr mutations significantly perturb the PI-PLC structure as judged by far-UV circular dichroism (CD), and all of the variants exhibit significant activity toward PI presented in small unilamellar vesicles (the preferred substrate) that increases as PC is added to the vesicle (see Supporting Information). In general, WT* PI-PLC and the Tyr* variants, (where the asterisk indicates the Asn168Cys mutation required for Cys-mediated fluorescent labeling of PI-PLC) have similar affinities for anionic SUVs containing only PG (Figure 5), and Tyr* defects in binding are greatest for SUVs with high X_{PC} . This is consistent with the simulations where most of the Tyr residues mediate interactions with choline headgroups.

For the loop between $\beta 2$ and helix D, mutagenesis of Tyr88 to Ala (Y88A*) increases the apparent K_d by at least 1 order of magnitude for $X_{PC} \geq 0.5$, while defects in binding of Y86A* are barely significant (Figure 5A). As might be expected, decreases in membrane affinity for the Y86A/Y88A* double mutant are dominated by the effect of mutating Tyr88. These results are consistent with the simulations where, compared to Tyr86, occupancies of cation- π interactions between Tyr88 and choline headgroups are much higher and are stabilized by additional interactions mediated by the phosphate group of the same lipid.

The Tyr residues in the helix F/helix G region can be broken into two groups: (i) the adjacent Tyr residues 246 and 247 on helix G, and (ii) Tyr204 on helix F as well as Tyr residues 248 and 251 on helix G. The Y246A* variant shows significant binding defects even at 0.2 X_{PC} (Figure 5C). Mutagenesis of Tyr247 is much less perturbing, and Y247A* has apparent K_d s that are only 5 times higher than WT* at $X_{PC} \geq 0.8$, where Y246A* has apparent K_d s more than 60 times larger than WT*. As expected from these results, the double mutant, Y246A/Y247A*, has reduced binding affinity similar to that seen for Y246A*. Again, this mirrors the simulations where Tyr246 cation- π interactions have high occupancies and are supported by a stable hydrogen bond mediated by S244, while Y247 mediates fewer cation- π interactions.

The results for Tyr residues 204, 248, and 251 are more complicated. The Tyr204 and Tyr251 variants behave similarly (Figure 5D). Mutagenesis of either Tyr residue has no significant effect on binding at $X_{PC} = 0$ or 0.2 but increases the apparent K_d by 5-fold for 0.5 X_{PC} and at least an order of

magnitude for vesicles with higher PC content. Additionally, the double mutant behaves similarly to either single mutant suggesting that the effects of these two mutations are not additive. In both the *S. aureus* N254Y/H258Y variant structure³¹ (where *S. aureus* PI-PLC residues 254 and 258 correspond to *B. thuringiensis* PI-PLC residues 247 and 251, respectively) and in the simulations with DMPC, Tyr residues corresponding to *B. thuringiensis* 204 and 251 interact with the same choline ion diffused into the crystal. Thus, the mutagenesis data with the Bacillus PI-PLC suggest that disrupting one of these interactions may be sufficient to disrupt the other.

Mutating Tyr residues 88, 246, or 248 has the largest effects on binding (Figure 5). However, unlike 88 and 246, the simulations predict that Tyr248 does not interact with the membrane but rather restricts conformations of the PI-PLC rim loop by interactions with other amino acids. The serious losses in binding affinity for the Y248A* variant when $X_{PC} > 0$ (Figure 5D) suggest that either the simulation underestimates the extent of interactions between 248 and lipids or the change in rim loop dynamics observed in the protein-only simulations for Y248A reduces binding affinity particularly for PC-rich vesicles.

DISCUSSION

This combination of simulations and experiments details the molecular mechanisms PI-PLC uses to bind PC-rich membranes. Simulations with an implicit membrane model yield an orientation of *B. thuringiensis* PI-PLC in good agreement with experimental data, even though the model significantly underestimates the energetic contribution of aromatic amino acids and possibly the overall binding energy. The all-atom simulation with a DMPC bilayer predicts specific interactions between individual PI-PLC residues and lipids. Two 500 ns simulations were also performed using a DMPC/DMPG 4:1 lipid bilayer and starting with different lipid distribution around the protein but almost identical PI-PLC orientations relative to the membrane. The occupancies and interactions between PC lipids and PI-PLC residues (data not shown) are not significantly different from those obtained with a pure PC bilayer. These results support the significance of the data obtained from the 500 ns-long DMPC simulation and suggest that these interactions are likely to occur for a variety of PC-rich bilayers.

Mutagenesis of the amino acids involved in the specific interactions observed during the simulation generally reduces PI-PLC affinity for lipid vesicles, validating the simulation results. In particular the importance of helix B seen in the simulations is in agreement with PI-PLC binding data toward SUVs.²⁰ The I43A mutant has an apparent K_d ~5.5 times greater than the WT protein. Mutating Lys44 to alanine increases K_d by more than 1 order of magnitude (cf. Supporting Information). In addition to helix B, containing the amino acids that are most deeply anchored in the bilayer, two other regions carry amino acids that interact with the lipid tails via hydrophobic interactions: the loop between $\beta 2$ and helix D and the loop between $\beta 7$ and helix G (rim loop region). Among all the interactions identified along the simulation, we observe a strikingly high number of interactions involving aromatic residues and in particular conformations of choline groups and tyrosine side chains characteristic of cation- π interactions. Again, mutagenesis of these Tyr residues reduces membrane affinity, particularly for PC-rich membranes.

The fact that FCS experiments show the greatest binding defects for vesicles with high PC/PG ratio confirms that tyrosines play an important role in specific PC, or at least choline, binding. Mutagenesis of tyrosines 88, 204, 246, and 251 increases the apparent K_d by at least an order of magnitude compared to WT PI-PLC. These are also the tyrosines for which we observe the highest number of cation- π occurrences during the MD simulation, suggesting that the cation- π interactions observed in the simulation are relevant for binding.

In contrast, mutagenesis of Tyr248 also reduces the apparent K_d by 2 orders of magnitude at high X_{PC} (Table 2), but barely any cation- π adduct is formed during the 500 ns simulation. While we cannot exclude that the simulations underestimate lipid-Tyr interactions, the intramolecular hydrophobic interactions of Tyr248 in the PI-PLC/DMPC simulation and the simulation of the Y248A mutant in water indicate that Tyr248 may help maintain the structure and rigidity of the rim loop region. In previous MD simulations on PI-PLC in solution, this rim loop (residues 238–244) was observed to open and close over the active site in concert with the helix B region.³³ Mutagenesis of Pro245 at the top of helix G resulted in a loss of this correlated motion in MD simulations, and Pro245 mutants show both reduced enzymatic activity and reduced binding affinity particularly toward PC-rich SUVs.³³ Taken all together the current and previous simulations along with helix G mutations suggest that the dynamics and orientation of the rim loop are important for PI-PLC activity and binding in PC-rich environments, such as the outer membrane of eukaryotic cells.

The energetics of Tyr/PC cation- π interactions are reflected in the occupancies observed during the simulations (Figure 3A) and may also be estimated by calculating $\Delta\Delta G$ ($= \Delta G_{\text{mutant}} - \Delta G_{\text{WT}}$) from the apparent K_d s for the Tyr mutants. Both of these methods only estimate the energetics because cation- π interactions may be underestimated in MD simulations (see below), and the apparent K_d s are calculated based on the total lipid concentrations rather than the lipid concentration in the SUV outer leaflet. (We chose to use the total lipid concentration because the SUVs used for the binding experiments are polydisperse,²¹ complicating estimates of the lipid concentration in the outer leaflet.) Despite these caveats, the cation- π occupancies and $\Delta\Delta G$ s calculated from the apparent K_d s are reasonably well-correlated for the 500 ns simulation (Figure 6). With the exception of Tyr248, the most

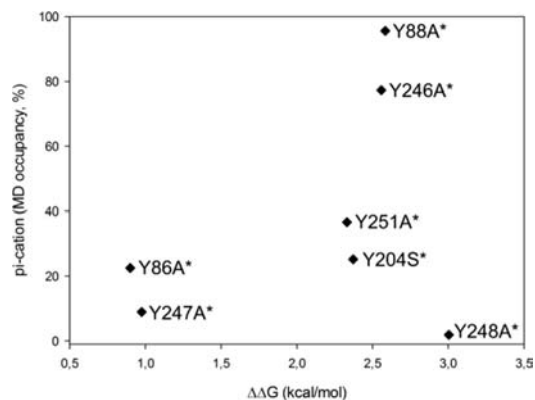


Figure 6. Comparison between occupancies of predicted cation- π interactions from the simulation and evaluation of $\Delta\Delta G$ (kcal/mol) from FCS measurements for PI-PLC WT* and single tyrosine mutants.

perturbing mutations (high $\Delta\Delta G$) are associated with Tyr residues exhibiting long cation- π occupancies indicating that the simulation does a good, qualitative job of modeling interactions between PC and Tyr residues.

Comparing the $\Delta\Delta G$ calculated from the apparent K_d values can also provide qualitative information about the type of interaction between tyrosines and PC. The free energy change associated with Tyr86 and Tyr247 is approximately -1 kcal/mol. This value is comparable to that predicted by the Wimley-White scale (0.94 ± 0.06 kcal/mol for the transfer of tyrosines³⁴ from water to 1-palmitoyl-2-oleoyl-phosphatidylcholine (POPC)) and in the range of a hydrogen-bonded interaction.³⁵ It is also close to the Wimley-White scale for transfer to octanol (-0.71 ± 0.11 kcal/mol) which reflects hydrophobic interactions. In contrast, removal of tyrosines 88, 204, 246, or 251 is linked to a higher energy cost: 2.5–3 kcal/mol toward pure PC vesicles. These higher energies may indicate cation- π interactions. Gallivan and Dougherty report an estimated upper limit of -3.6 kcal/mol for a methylammonium-benzene cation- π interaction.³⁵ Altogether, these results strongly indicate the presence of these cation- π interactions.

Some of the most important cation- π interactions are also correlated with strong hydrogen bonds (Lys44, Ser244), suggesting a network of interactions at the interfacial binding site involving the cation- π interactions. However, longer MD simulations would be needed to confirm the stability of this network.

To the best of our knowledge, investigations of cation- π interactions between membrane proteins and lipids have so far mostly focused on tryptophans. While the two tryptophan residues present at the PI-PLC binding interface are deeply anchored and interact mostly with the hydrophobic lipid chains, we observe cation- π interactions mediated almost exclusively by tyrosines. This is in agreement with protein structures^{5–9} and studies on simpler systems, both experimental and theoretical, that provide evidence for the existence of cation- π adducts between tetramethylammonium or choline moieties and phenolic groups of tyrosine.

Cation- π interactions result from electrostatic interactions between π electrons of an aromatic system, in proteins typically Phe, Tyr or Trp, and a cation (e.g., $-\text{NH}_3^+$, $-\text{N}(\text{CH}_3)_3^+$). The origin of the dominating component (electrostatic interaction with the quadrupole, polarization of the aromatic system, charge transfer, dispersion effects) has been debated over the years. Although several studies argue for a dominant electrostatic contribution,^{1,36–38} other studies have concluded that the other contributions cannot be overlooked.^{39,40} Whichever scenario we envisage, there are good reasons to doubt the ability of additive pairwise potentials from molecular mechanics force field to accurately reproduce the energetics of cation- π interactions.^{10,41} Yet molecular mechanics force fields have been shown to capture geometries of cation- π pairs in proteins fairly well.^{41,42} Our work expands previous results and suggests that the Charmm force field provides a qualitatively reasonable picture of the cation- π interactions between PI-PLC and phosphatidylcholine lipids. However, we cannot exclude that our simulation misses or underestimates some interactions, such as the formation of cages of Tyr residues as recently observed for *S. aureus* PI-PLC.^{31,43} This could be caused by the fact that positive charges approaching along the plane of the aromatic ring are not well described by Charmm.³⁷ Yet the qualitatively good agreement between the simulation and the

FCS experiments reported here indicate that MD simulations with a classical mechanics force field have strong predictive power for protein–lipid interfacial interactions, even when they involve “challenging” adducts, such as the cation– π systems.

The binding affinity between membrane lipids and amphitropic proteins is typically the result of interfacial interactions, most often referred to as the sum of electrostatics (hydrogen bonds) between basic amino acids (Lys, Arg) and the interface (phospholipid heads) and hydrophobic interactions of aliphatic amino acids with the lipid tails. The role of interfacial aromatic amino acids is seldom mentioned despite the importance of these residues. Our results suggest that tyrosine residues are involved in interfacial cation– π interactions that are potentially energetically equivalent to or stronger than hydrophobic interactions or hydrogen bonds. It has been suggested that cation– π interactions are less sensitive to the solvent dielectric constant than salt bridges³⁵ making them well-adapted for the interface between a low and a high dielectric environment. Moreover other phospholipids have amino groups capable of interacting with aromatic systems. PE is abundant in bacteria, and phosphatidylserine distribution between the inner and outer leaflet of eukaryotic plasma membranes is modified in apoptotic cells. Our results suggest that overlooked cation– π interactions between membranes and aromatic amino acids of amphitropic proteins may play an important role not only in membrane binding but also in lipid specificity.

CONCLUSION

Experimental mutagenesis of PI-PLC Tyr residues implicated in cation– π interactions with PC revealed an excellent correlation between the occupancy of cation– π interactions in the MD simulation and the severity of binding defects in the Tyr variants. This relationship did not hold for Tyr248 which is instead implicated in constraining protein intrinsic dynamics that are critical for membrane binding as suggested recently.²³ This study also presents a semiquantitative analysis of the energetics of choline-tyrosine cation– π interactions in protein–membrane binding suggesting that strong cation– π interactions may provide up to 3 kcal/mol of binding energy at the interface. It demonstrates the utility of relatively long protein plus membrane simulations using molecular mechanics force fields for insight into the molecular mechanisms used for membrane binding by amphitropic proteins including both amino acid–lipid interactions and possible roles for protein dynamics. Cation– π interactions between aromatic residues, including tyrosines, and the interfacial membrane region may be an overlooked, important mechanism utilized by other amphitropic proteins with aromatic rich regions.

METHODS

MD Simulations. *Simulations with an Implicit Membrane Model.* There is no X-ray structure of WT *B. thuringiensis* PI-PLC. We thus used the X-ray structure of the *B. thuringiensis* Y247S/Y251S²² mutant (PDB ID: 3EA1) for which we constructed the missing tyrosine side chains using the X-ray structure of the W47A/W242A⁴⁴ mutant (PDB ID: 2OR2). The obtained structure was then subjected to an energy minimization using harmonic restraints (50 kcal/mol/Å² on the backbone and 15 kcal/mol/Å² on side chains) using Charmm (v33b1).⁴⁵ Simulations with the IMM1-GC implicit membrane model^{27,28} were also performed with Charmm (v33b1),⁴⁵ using a salt concentration of 0.1 M, a membrane thickness of 23 Å, an area per lipid of 70 Å² and a 50% ratio of anionic “lipid” of valence 1. The plane of smeared charge was positioned 3 Å above the membrane

plane (i.e., at $z = \pm 14.5$ Å). The Charmm polar hydrogen force field⁴⁶ was used to describe the protein. The simulations were run for 4 ns and, as described previously,²⁹ starting from six different orientations of the proteins with respect to the membrane. Each orientation corresponds to one face of a cube containing the protein and was used as a starting point for three independent simulations using different distributions of the initial velocities. The conformations were stored every picosecond. For each stored conformation we calculated the effective energy of the enzyme in water, using the EEF1.1 force field.²⁷ The binding energy of PI-PLC to membranes could thus be calculated every picosecond as the difference between the effective energy with the membrane model IMM1-GC and the effective energy in water (EEF1.1) (as described in detail in ref 29). The structural and energetic analyses were done on the simulation that led to the lowest average effective energy. The trajectory between 2.5 and 4 ns was used for analysis as the anchorage depth and binding energy were stable on this time scale. Note that we also ran the same simulations with a neutral implicit bilayer, but these did not lead to significant anchorage of PI-PLC (data not shown). IMM1 generally underestimates the binding of PI-PLC, both with zwitterionic and anionic membranes presumably because it underestimates the nonhydrophobic contribution of aromatic amino acids. The contributions of each PI-PLC amino acid to the solvation free energy were calculated for every frame in the last 1.5 ns of the simulation and then averaged. We then calculated the difference with the corresponding terms in water to evaluate the contribution of each atom to the membrane binding energy. The atomic contributions were summed to obtain residue contributions.

Simulation with an Explicit Bilayer. The last 3 ns of the three IMM1 simulations leading to membrane anchorage were merged to evaluate the backbone angle and center of gravity. We then selected the conformation that had the orientation with the lowest deviations relative to the average binding energy values, angle as well as center of gravity, and used it to initiate the all-atom simulation. Only the orientation and not the protein structure was used since long implicit solvent simulations can result in high protein flexibility and unrealistic deformations. Instead a combination of X-ray structures 2OR2 and 3EA1 was used (see above) and oriented following the IMM1 results. The bilayer contains 256 DMPC lipids. It was taken from Broemstrup et al.⁴⁷ and further equilibrated for 100 ns with the Charmm36 force field²³ (average value of surface area per lipid was 60.9 ± 0.9 Å²). In order to reduce steric clashes, four lipids were removed after insertion of the protein into the leaflet. Membrane and protein were then submitted to an energy minimization using the following harmonic restraints: 150 kcal/mol/Å² for protein backbone and water molecules; 100 kcal/mol/Å² for membrane atoms located further than 5 Å from the protein and protein side chain atoms located further than 5 Å from the membrane; 50 kcal/mol/Å² for membrane atoms located within 5 Å of the protein; 15 kcal/mol/Å² for protein side chains atoms located 5 Å or less from the membrane. The minimization consisted of 20 consecutive cycles of 600 minimization steps (500 steepest descent, 100 conjugated gradients) with restraints being scaled by 0.65 after each cycle. TIP3P water molecules were then added to the minimized structure using VMD⁴⁸ which resulted in a system with dimension $80 \times 90 \times 115$ Å. Finally, we replaced seven water molecules, chosen randomly by sodium ions to neutralize the system.

The program NAMD(v2.9)⁴⁹ was used to perform the simulations at 310 K with an integration time step of 2 fs, in the NPT ensemble, without surface tension in the isobaric–isothermal ensemble using the Langevin piston method⁵⁰ (target pressure: 1 atm, oscillation period: 200 fs, damping time scale: 50 fs) and Langevin dynamics to control the temperature (temperature damping coefficient: 1.0). We used the Charmm force field⁵¹ (c27 including the CMAP corrections⁵²) with the force field update for lipids (Charmm36).²³ The equations of motion were integrated using a multiple time step algorithm;⁵³ bonded interactions and short-range nonbonded forces were evaluated every step, and long-range electrostatics every second step. Force-based switching was used for both electrostatic and van der Waals interactions, with a switch distance of 11 Å and a cutoff of 12 Å. Particle mesh Ewald⁵⁴ was used for long-range electrostatic interactions. SHAKE⁵⁵ was applied to constrain all bonds between

hydrogen and heavy atoms. We first performed two short initial equilibrations of 400 ps each in the NVT ensemble, velocities being reassigned every 100 fs and 1 ps, respectively, with a constrained protein backbone. Constraints were then removed, and the system was further equilibrated for 2 ns with periodic reassignment of the velocities every 1 ps. The production phase was finally run for 500 ns. Backbone RMSD compared to the minimized X-ray structure was monitored and revealed an overall stable structure of PI-PLC.

Simulations in Water. The WT enzyme and the Y248A mutant were simulated in TIP3P water. The starting structure was the same as above, and the procedure similar except for the heating/equilibration procedure. The structures were first submitted to four successive heating stages of 2 ps each at 10, 100, 200, and 300 K, respectively. The equilibration procedure was 200 ps long with a velocity reassignment every picosecond. A time step of 1 fs and a simulation temperature of 300 K were used. The systems were solvated in boxes of $90 \times 90 \times 90 \text{ \AA}$.

Trajectory Analysis. Analyses presented here were performed on the whole trajectory minus the first 50 nanoseconds (450 ns). The only exception is the calculation of depth of anchorage which is done over the whole simulation.

Hydrophobic contacts are considered to exist if two unbound candidate atoms are within 3 \AA for at least 10 ps. Candidate atoms are atoms in aliphatic groups of amino acids side chains (Charmm force field nomenclature: ca; cb; cg1; cg2; ha*; hb*; hg; hg2*; type cg except the one of hsd, hse, asn, asp; type hg1 except for cys, thr, ser; type cd except for arg, gln glu; type cd1; type cd2 except for hsd, hse; type ce1, ce2, cz and associated hydrogens of phe, tyr; type cd1, cd2, ce2, ce3, cz2, cz3 and associated hydrogens of trp; type cay and type hy*). The criteria for hydrogen bonds are the following: acceptor (A) to hydrogen distance $\leq 2.4 \text{ \AA}$ and angle D–H–A (D: hydrogen-bond donor) $\geq 130^\circ$. These two criteria must be met for at least 10 ps. The donor and acceptor definitions are from the Charmm⁵¹ force field. Cation– π interactions between the aromatic rings of tyrosines and tryptophans were considered to exist when all distances between the aromatic ring atoms and the choline nitrogen were below 7 \AA . Additionally these distances should not differ by more than 1.5 \AA .^{10,42} We report occupancies (number of trajectory conformations where the interaction is present/total number of conformations) for cation– π interactions and hydrogen bonds. We chose to report the average number of contacts per frame for hydrophobic interactions because a given residue can mediate several interactions at a time, and reporting occupancies would not reflect the number of interacting partners. Hydrogen bonds and cation– π interactions on the other hand rarely involve more than one simultaneous partner. Due to lipid diffusion, a given residue can interact with different DMPC molecules along the simulation, but we consider the membrane as a whole and lipids as interchangeable. Time-evolution plots of cation– π interactions (Figure 3A), hydrogen bonds, and hydrophobic contacts (Figure 1, Supporting Information) provide insight into the stability of the main interactions. These plots are generated as follows: the simulation is divided into 1 ns-long windows, and one dot is plotted if the interaction/contact is observed on at least half of the conformations of the window centered around that point.

To evaluate the depth of anchorage, we used the average z coordinate of the phosphorus atoms as a reference (the plane of the membrane is perpendicular to the z axis). For each frame, the z coordinate of the center of mass of each residue was calculated, and its distance to the reference was measured. All coordinates statistics were done using the corman module of the Charmm program. Values reported are averages of the distances calculated over the whole simulation. Plots along simulation time of RMSD, occupancies of hydrogen bonds, number of hydrophobic contacts, and depth of anchorage are provided as Supporting Information.

Enzyme Expression and Purification. All PI-PLC mutants were constructed in the N168C *B. thuringiensis* PI-PLC background using QuikChange methodology with a site-directed mutagenesis kit (Agilent Technologies). The salt-free purified mutagenic primers were purchased from Operon. All mutated genes were sequenced at Genewiz to confirm that the desired mutation was introduced. A

plasmid containing the mutant *B. thuringiensis* gene was transformed into *Escherichia coli* BL21-Codonplus (DE3)-RIL cells. Overexpression and purification of these mutants followed procedures described previously.¹⁹ These mutants expressed well in *E. coli*, and >90% purity of isolated protein, as monitored by SDS-PAGE, was achieved by chromatography on a Q-Sepharose fast flow column followed by a phenyl-Sepharose column as described for the recombinant *B. thuringiensis* PI-PLC (rPI-PLC).¹⁹ Protein solutions were concentrated using Millipore Central plus 10 filters, and concentrations were estimated by absorption at 280 nm using the extinction coefficient calculated using ProtParam.⁵⁶ Secondary structure, as estimated from far UV CD data using an AVIV 202 CD spectrophotometer, was essentially the same for all the single tyrosine mutants indicating no significant change in secondary structure. Small changes were seen for some of the double mutants, but these were close to the error in the deconvolution of the spectra, performed using the CDNN program⁵⁷ (see Supporting Information). Thermal stability of PI-PLC variants was assessed by monitoring the ellipticity at 222 nm while increasing the sample temperature $0.5^\circ/\text{min}$.^{20,33} Activities for all the variants (see Supporting Information), determined toward 4 mM PI in small vesicles with various amounts of PC, were determined by ³¹P NMR spectroscopy as described previously.^{21,30}

Preparation of SUVs. Stock solutions of POPC and dioleoyl-phosphatidylglycerol in chloroform were purchased from Avanti Polar Lipids. SUVs with increasing mole fractions of POPC were prepared by sonication in phosphate buffered saline (PBS), pH 7.4, as previously described.³²

Measuring PI-PLC Binding to SUVs with FCS. The FCS-based SUV binding experiments take advantage of the fact that protein binding to vesicles slows translational diffusion. FCS experiments were performed using PI-PLC variants labeled at N168C with Alexa Fluor 488 maleimide and a home-built confocal setup based on an IX-70 inverted microscope (Olympus) as previously described.³² FCS experiments were carried out at 22°C on $300 \mu\text{L}$ samples in PBS, pH 7.4, plus 1 mg/mL bovine serum albumin (BSA) to stabilize PI-PLC, in chambered coverglass wells (LabTek) coated with 10 mg/mL BSA and rinsed with PBS prior to use to prevent protein adhesion to the sides of the wells. Ten nM labeled PI-PLC was titrated with unlabeled SUVs, and the fraction of protein bound to vesicles was determined from two species fits to the autocorrelations (obtained in crosscorrelation mode), $G(\tau)$ ^{33,58–60}

$$G(\tau) = A_p g_p(\tau) + A_v g_v(\tau) \quad (1)$$

Where p and v denote free protein and SUVs that are fluorescent due to PI-PLC binding, respectively, and A_j is the amplitude of species j . The correlation function for species j , $g_j(\tau)$, accounts for diffusion of the molecules through the observation volume which depends on the radius and extent of the observation volume, determined from fits to rhodamine 110 calibration data using $D = 280 \mu\text{m}^2 \text{ s}^{-1}$ at 22°C ,⁶¹ and D_p , the diffusion coefficient for each species.^{58,62} D_p for the free protein was experimentally determined in the absence of vesicles, while D_v for the SUVs was determined from global fits to all of the titration experiments for a particular X_{PC} using Origin (OriginLab). The apparent fraction of protein bound to the SUVs, f , can be determined from A_p and the time-averaged number of proteins in the observation volume in the absence of vesicles,^{59,60} $\langle N_{p,0} \rangle$:

$$f = 1 - A_p / \langle N_{p,0} \rangle = 1 - A_p / A_{p,0} \quad (2)$$

where $A_{p,0} = 1 / \langle N_{p,0} \rangle$ is the autocorrelation amplitude for free PI-PLC prior to titration corrected for volume changes. The apparent dissociation constant, K_d , representing PI-PLC partitioning to the vesicle surface, and a cooperativity coefficient, n , was determined from fits to a Hill equation:

$$f = f_{\text{max}} [\text{PL}]^n / (K_d^n + [\text{PL}]^n) \quad (3)$$

where f , is determined for different total lipid concentrations, $[\text{PL}]$, at fixed X_{PC} , and f_{max} is the apparent maximum fraction bound. Fitting the correlation curves to eq 1 assumes that all of the SUVs have a single well-defined radius with a single diffusion coefficient. However

the SUVs are not a single population but rather have a distribution of sizes. Fitting a polydisperse population to a single size, using eq 1, has no significant effects on the value for the apparent K_d but does reduce the value of f_{\max} (see the Supporting Information for refs 21 and 63). Reductions in the apparent fraction bound mean that even in the case of 100% binding, the value of f_{\max} determined from fits to eq 3 is less than one. FCS experiments were repeated twice using different vesicle and protein preparations. Assuming that uncertainties are normally distributed, we consider a change of 3 times the standard deviation in apparent K_d to be significant. Based on this assumption and the standard deviation values from all of the FCS measurements, a 2–3 times increase in apparent K_d relative to N168C PI-PLC (WT*) is considered significant.

■ ASSOCIATED CONTENT

■ Supporting Information

Implicit membrane energy decomposition per amino acid (Table 1); RMSD, depth of anchorage, hydrogen bonds, and hydrophobic contacts along simulation time (Figure 1); RMSF from simulations of WT and Y248A in water (Figure 2); activity (Figure 3) and far UV CD data (Table 2) for WT* (N168C) and double Tyr variants of PI-PLC Binding affinities of the K44A* variant to PG/PC SUVs as a function of mole fraction of PC (Figure 4). This material is available free of charge via the Internet at <http://pubs.acs.org>.

■ AUTHOR INFORMATION

Corresponding Author

nathalie.reuter@mbi.uib.no

Notes

The authors declare no competing financial interest.

■ ACKNOWLEDGMENTS

This work was supported by grants from the Bergen Research Foundation to N.R. and C.G. and by the National Institute of General Medical Sciences of the National Institutes of Health under award no. R01GM060418 to M.F.R. Parallab (High Performance Computing Laboratory at the University of Bergen) and NOTUR (Norwegian metacenter for computational science) are thankfully acknowledged for provision of CPU time.

■ REFERENCES

- (1) Ma, J. C.; Dougherty, D. A. *Chem Rev* **1997**, *97*, 1303–1324.
- (2) Mahadevi, A. S.; Sastry, G. N. *Chem Rev* **2013**, *113*, 2100–2138.
- (3) Xiu, X.; Puskas, N. L.; Shanata, J. A.; Lester, H. A.; Dougherty, D. A. *Nature* **2009**, *458*, 534–7.
- (4) Gallivan, J. P.; Dougherty, D. A. *Proc. Natl. Acad. Sci. U.S.A.* **1999**, *96*, 9459–64.
- (5) Roderick, S. L.; Chan, W. W.; Agate, D. S.; Olsen, L. R.; Vetting, M. W.; Rajashankar, K. R.; Cohen, D. E. *Nat. Struct. Biol.* **2002**, *9*, 507–511.
- (6) Beene, D. L.; Brandt, G. S.; Zhong, W.; Zacharias, N. M.; Lester, H. A.; Dougherty, D. A. *Biochemistry* **2002**, *41*, 10262–9.
- (7) Celie, P. H. N.; van Rossum-Fikkert, S. E.; van Dijk, W. J.; Brejc, K.; Smit, A. B.; Sixma, T. K. *Neuron* **2004**, *41*, 907–914.
- (8) Pittelkow, M.; Tschapek, B.; Smits, S. H.; Schmitt, L.; Bremer, E. *J. Mol. Biol.* **2011**, *411*, 53–67.
- (9) Tschapek, B.; Pittelkow, M.; Sohn-Bosser, L.; Holtmann, G.; Smits, S. H.; Gohlke, H.; Bremer, E.; Schmitt, L. *J. Mol. Biol.* **2011**, *411*, 36–52.
- (10) Petersen, F. N. R.; Jensen, M. O.; Nielsen, C. H. *Biophys. J.* **2005**, *89*, 3985–3996.
- (11) Aliste, M. P.; MacCallum, J. L.; Tieleman, D. P. *Biochemistry* **2003**, *42*, 8976–8987.

- (12) de Jesus, A. J.; Allen, T. W. *Biochim. Biophys. Acta* **2013**, *1828*, 864–76.
- (13) Broemstrup, T.; Reuter, N. *Phys. Chem. Chem. Phys.* **2010**, *12*, 7487–96.
- (14) Sanderson, J. M. *Org. Biomol. Chem.* **2007**, *5*, 3276–3286.
- (15) Sanderson, J. M.; Whelan, E. J. *Phys. Chem. Chem. Phys.* **2004**, *6*, 1012–1017.
- (16) Johnson, J. E.; Cornell, R. B. *Mol. Membr. Biol.* **1999**, *16*, 217–235.
- (17) Kim, J. Y.; Mosior, M.; Chung, L. A.; Wu, H.; Mclaughlin, S. *Biophys. J.* **1991**, *60*, 135–148.
- (18) Luckey, M. *Membrane Structural Biology: With Biochemical and Biophysical Foundations*; Cambridge University Press: Cambridge, 2008.
- (19) Feng, J.; Wehbi, H.; Roberts, M. F. *J. Biol. Chem.* **2002**, *277*, 19867–75.
- (20) Guo, S.; Zhang, X.; Seaton, B. A.; Roberts, M. F. *Biochemistry* **2008**, *47*, 4201–10.
- (21) Pu, M.; Roberts, M. F.; Gershenson, A. *Biochemistry* **2009**, *48*, 6835–45.
- (22) Shi, X.; Shao, C.; Zhang, X.; Zambonelli, C.; Redfield, A. G.; Head, J. F.; Seaton, B. A.; Roberts, M. F. *J. Biol. Chem.* **2009**, *284*, 15607–18.
- (23) Klauda, J. B.; Venable, R. M.; Freites, J. A.; O'Connor, J. W.; Tobias, D. J.; Mondragon-Ramirez, C.; Vorobyov, I.; MacKerell, A. D., Jr.; Pastor, R. W. *J. Phys. Chem. B* **2010**, *114*, 7830–43.
- (24) Heinz, D. W.; Ryan, M.; Bullock, T. L.; Griffith, O. H. *EMBO J.* **1995**, *14*, 3855–63.
- (25) Baker, N. A.; Sept, D.; Joseph, S.; Holst, M. J.; McCammon, J. A. *Proc. Natl. Acad. Sci. U.S.A.* **2001**, *98*, 10037–10041.
- (26) Rogaski, B.; Klauda, J. B. *J. Mol. Biol.* **2012**, *423*, 847–61.
- (27) Lazaridis, T. *Proteins* **2003**, *52*, 176–92.
- (28) Lazaridis, T. *Proteins* **2005**, *58*, 518–27.
- (29) Hajjar, E.; Mihajlovic, M.; Witko-Sarsat, V.; Lazaridis, T.; Reuter, N. *Proteins* **2008**, *71*, 1655–1669.
- (30) Pu, M.; Orr, A.; Redfield, A. G.; Roberts, M. F. *J. Biol. Chem.* **2010**, *285*, 26916–22.
- (31) Goldstein, R. I. Ph.D. dissertation, Boston College: Chestnut Hill, MA, 2012.
- (32) Pu, M.; Fang, X.; Redfield, A. G.; Gershenson, A.; Roberts, M. F. *J. Biol. Chem.* **2009**, *284*, 16099–107.
- (33) Cheng, J.; Karri, S.; Grauffel, C.; Wang, F.; Reuter, N.; Roberts, M. F.; Wintrode, P. L.; Gershenson, A. *Biophys. J.* **2013**, *104*, 1–11.
- (34) Wimley, W. C.; Creamer, T. P.; White, S. H. *Biochemistry* **1996**, *35*, 5109–5124.
- (35) Gallivan, J. P.; Dougherty, D. A. *J. Am. Chem. Soc.* **2000**, *122*, 870–874.
- (36) Dougherty, D. A. *Science* **1996**, *271*, 163–8.
- (37) Kumpf, R. A.; Dougherty, D. A. *Science* **1993**, *261*, 1708–10.
- (38) Luhmer, M.; Bartik, K.; Dejaegere, A.; Bovy, P.; Reisse, J. *Bull. Soc. Chim. Fr.* **1994**, *131*, 603–606.
- (39) Caldwell, J. W.; Kollman, P. A. *J. Am. Chem. Soc.* **1995**, *117*, 4177–4178.
- (40) Yau, W. M.; Wimley, W. C.; Gawrisch, K.; White, S. H. *Biochemistry* **1998**, *37*, 14713–8.
- (41) Woolf, T. B.; Grossfield, A.; Pearson, J. G. *Int. J. Quantum Chem.* **1999**, *75*, 197–206.
- (42) Minoux, H.; Chipot, C. *J. Am. Chem. Soc.* **1999**, *121*, 10366–10372.
- (43) Goldstein, R.; Cheng, J.; Stec, B.; Roberts, M. F. *Biochemistry* **2012**, *51*, 2579–87.
- (44) Shao, C.; Shi, X.; Wehbi, H.; Zambonelli, C.; Head, J. F.; Seaton, B. A.; Roberts, M. F. *J. Biol. Chem.* **2007**, *282*, 9228–35.
- (45) Brooks, B. R.; Brooks, C. L., III; Mackerell, A. D., Jr.; Nilsson, L.; Petrella, R. J.; Roux, B.; Won, Y.; Archontis, G.; Bartels, C.; Boresch, S.; Cafisch, A.; Caves, L.; Cui, Q.; Dinner, A. R.; Feig, M.; Fischer, S.; Gao, J.; Hodoscek, M.; Im, W.; Kuczera, K.; Lazaridis, T.; Ma, J.; Ovchinnikov, V.; Paci, E.; Pastor, R. W.; Post, C. B.; Pu, J. Z.; Schaefer, M.; Tidor, B.; Venable, R. M.; Woodcock, H. L.; Wu, X.

Yang, W.; York, D. M.; Karplus, M. *J. Comput. Chem.* **2009**, *30*, 1545–614.

(46) Neria, E.; Fischer, S.; Karplus, M. *J. Chem. Phys.* **1996**, *105*, 1902–1921.

(47) Broemstrup, T.; Reuter, N. *Biophys. J.* **2010**, *99*, 825–33.

(48) Humphrey, W.; Dalke, A.; Schulten, K. *J. Molec. Graphics* **1996**, *14*, 33–38.

(49) Phillips, J. C.; Braun, R.; Wang, W.; Gumbart, J.; Tajkhorshid, E.; Villa, E.; Chipot, C.; Skeel, R. D.; Kale, L.; Schulten, K. *J. Comput. Chem.* **2005**, *26*, 1781–802.

(50) Feller, S. E.; Zhang, Y. H.; Pastor, R. W.; Brooks, B. R. *J. Chem. Phys.* **1995**, *103*, 4613–4621.

(51) MacKerell, A. D.; Bashford, D.; Bellott, M.; Dunbrack, R. L.; Evanseck, J. D.; Field, M. J.; Fischer, S.; Gao, J.; Guo, H.; Ha, S.; Joseph-McCarthy, D.; Kuchnir, L.; Kuczera, K.; Lau, F. T. K.; Mattos, C.; Michnick, S.; Ngo, T.; Nguyen, D. T.; Prodhom, B.; Reiher, W. E.; Roux, B.; Schlenkrich, M.; Smith, J. C.; Stote, R.; Straub, J.; Watanabe, M.; Wiorkiewicz-Kuczera, J.; Yin, D.; Karplus, M. *J. Phys. Chem. B* **1998**, *102*, 3586–3616.

(52) Mackerell, A. D.; Feig, M.; Brooks, C. L. *J. Comput. Chem.* **2004**, *25*, 1400–1415.

(53) Izaguirre, J. A.; Reich, S.; Skeel, R. D. *J. Chem. Phys.* **1999**, *110*, 9853–9864.

(54) Essmann, U.; Perera, L.; Berkowitz, M. L.; Darden, T.; Lee, H.; Pedersen, L. G. *J. Chem. Phys.* **1995**, *103*, 8577–8593.

(55) Andersen, H. C. *J. Comput. Phys.* **1983**, *52*, 24–34.

(56) Gasteiger, E.; Hoogland, C.; Gattiker, A.; Duvaud, S.; Wilkins, M. R.; Appel, R. D.; Bairoch, A. In *The Proteomics Protocols Handbook*; Walker, J. M., Ed.; Humana Press: New York, 2005, 571–607.

(57) Bohm, G.; Muhr, R.; Jaenicke, R. *Protein Eng.* **1992**, *5*, 191–5.

(58) Thompson, N. L. In *Topics in Fluorescence Spectroscopy*; Lakowicz, J. R., Ed.; Plenum Press: New York, 1991, 337–378.

(59) Rusu, L.; Gambhir, A.; McLaughlin, S.; Radler, J. *Biophys. J.* **2004**, *87*, 1044–1053.

(60) Middleton, E. R.; Rhoades, E. *Biophys. J.* **2010**, *99*, 2279–2288.

(61) Magde, D.; Elson, E. L.; Webb, W. W. *Biopolymers* **1974**, *13*, 29–61.

(62) Elson, E. L.; Magde, D. *Biopolymers* **1974**, *13*, 1–27.

(63) Cheng, J.; Karri, S.; Grauffel, C.; Wang, F.; Reuter, N.; Roberts, M. F.; Wintrode, P. L.; Gershenson, A. *Biophys. J.* **2013**, *104*, 185–95.